



Published in final edited form as:

ACS Infect Dis. 2015 November 13; 1(11): 544–554. doi:10.1021/acsinfecdis.5b00046.

Bisthiazolidines: A Substrate-Mimicking Scaffold as an Inhibitor of the NDM-1 Carbapenemase

Mariano M. González[†], Magda Kosmopoulou[‡], Maria F. Mojica[§], Valerie Castillo[⊥], Philip Hinchliffe[‡], Ilaria Pettinati, Jürgen Brem, Christopher J. Schofield, Graciela Mahler[⊥], Robert A. Bonomo[§], Leticia I. Llarrull[†], James Spencer^{*,‡}, and Alejandro J. Vila^{*,†}

[†]Instituto de Biología Molecular y Celular de Rosario (IBR-CONICET), Facultad de Ciencias Bioquímicas y Farmacéuticas, Universidad Nacional de Rosario (UNR), Ocampo y Esmeralda, 2000 Rosario, Argentina

[‡]School of Cellular and Molecular Medicine, Medical Sciences Building, University of Bristol, University Walk, Bristol BS8 1TD, United Kingdom

[§]Research Service, Louis Stokes Cleveland Department of Veterans Affairs Medical Center, and Departments of Pharmacology, Biochemistry, Microbiology, and Molecular Biology, Case Western Reserve University, Cleveland, Ohio 44106, United States

[⊥]Laboratorio de Química Farmacéutica, Facultad de Química, Universidad de la República (UdelAR), Montevideo 11200, Uruguay

Department of Chemistry, University of Oxford, Chemistry Research Laboratory, 12 Mansfield Road, Oxford OX1 3TA, United Kingdom

Abstract

Pathogenic Gram-negative bacteria resistant to almost all β -lactam antibiotics are a major public health threat. Zn(II)-dependent or metallo- β -lactamases (MBLs) produced by these bacteria inactivate most β -lactam antibiotics, including the carbapenems, which are “last line therapies” for life-threatening Gram-negative infections. NDM-1 is a carbapenemase belonging to the MBL family that is rapidly spreading worldwide. Regrettably, inhibitors of MBLs are not yet developed. Here we present the bisthiazolidine (BTZ) scaffold as a structure with some features of β -lactam substrates, which can be modified with metal-binding groups to target the MBL active site. Inspired by known interactions of MBLs with β -lactams, we designed four BTZs that behave as in vitro NDM-1 inhibitors with K_i values in the low micromolar range (from 7 ± 1 to $19 \pm 3 \mu\text{M}$). NMR spectroscopy demonstrated that they inhibit hydrolysis of imipenem in NDM-1-producing *Escherichia coli*. In vitro time kill cell-based assays against a variety of bacterial strains harboring

*Corresponding Authors: (A.J.V.) vila@ibr-conicet.gov.ar. (J.S.) jim.spencer@bristol.ac.uk.

Accession Codes

The Protein Data Bank entry for the NDM-1/CS319 complex is 4U4L.

Notes

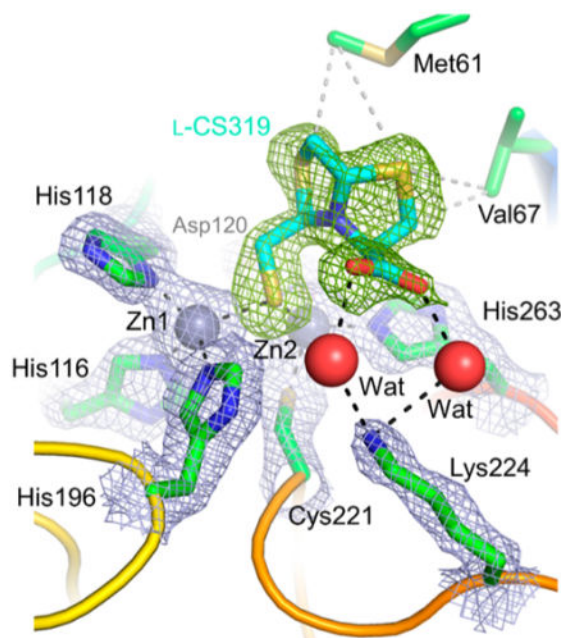
The authors declare no competing financial interest.

Supporting Information

The Supporting Information is available free of charge on the ACS Publications website at DOI: 10.1021/acsinfec-dis.5b00046. Supporting figures, scheme, and table (PDF)

*bla*_{NDM-1} including *Acinetobacter baumannii* show that the compounds restore the antibacterial activity of imipenem. A crystal structure of the most potent heterocycle (L-CS319) in complex with NDM-1 at 1.9 Å resolution identified both structural determinants for inhibitor binding and opportunities for further improvements in potency.

Graphical abstract



Keywords

antibiotic resistance; inhibitors; bisthiazolidines; metallo- β -lactamase; NDM-1

Seven decades after the clinical introduction of penicillin, β -lactam resistance is a major public health problem, a situation aggravated by overuse of this class of antibiotics in hospitals and agriculture. A succession of increasingly potent penicillins, cephalosporins, and carbapenems was developed, with carbapenems now often being used as “last-resort therapies” for the treatment of β -lactam-resistant bacterial infections.^{1–3} The therapeutic efficacy of carbapenem antibiotics (imipenem, meropenem, ertapenem, and doripenem) is severely challenged by the appearance and spread of carbapenemases in Gram-negative bacteria. Carbapenemases include two types of enzymes: (i) those with an essential Ser residue in their active site, known as serine- β -lactamases (SBLs), and (ii) the Zn(II)-dependent metallo- β -lactamases (MBLs). Whereas only a few SBLs (e.g., KPC-2^{4,5}) are capable of hydrolyzing carbapenems, most MBLs display an unusually broad substrate profile, being able to inactivate all bicyclic β -lactam antibiotics. The association of MBL genes with mobile genetic elements (and other resistance cassettes) facilitated the dissemination of these enzymes among prevalent pathogens such as *Pseudomonas aeruginosa* and members of the Enterobacteriaceae, making them serious clinical threats.^{6,7}

New Delhi metallo- β -lactamase-1 (NDM-1), originally found encoded by a multiresistance plasmid in *Klebsiella pneumoniae*,⁸ is one of the most widespread carbapenemases and has been identified in multiple pathogenic and environmental species⁷ on every inhabited continent. NDM-1 is a member of the B1 subclass of MBLs that represents the largest and most clinically relevant group of MBLs.

Crystal structures of NDM-1^{9–11} reveal a dinuclear metal center in the active site, composed of two Zn(II) ions (Figure 1): one containing a tetrahedral coordination sphere (Zn1 site) and one in a trigonal bipyramidal coordination sphere (Zn2 site). The Zn1 site consists of a Zn(II) ion coordinated to residues H116, H118, and H196 and a water/hydroxide molecule (we have used the standard BBL numbering scheme¹² throughout this paper). The metal ion at the Zn2 site is coordinated to residues D120, C221, and H263, a water molecule, and the formerly mentioned water/hydroxide. As with all MBLs, NDM-1 is not inhibited by commercially available (mechanism-based) serine- β -lactamase inhibitors, and clinically useful MBL inhibitors are not yet identified.^{13–16}

Several papers reveal thiol-bearing carboxylate compounds, such as D- and L-captopril,^{8,17–19} as well as carboxylate-bearing compounds such as a maleic acid derivative, ME1017,²⁰ and rhodanine-derived ene-thiolates²¹ as active NDM-1 inhibitors. Natural products have also been reported to inhibit NDM-1 by “sequestration” of the essential Zn(II) cofactors.²² Inspired by these attempts, here we report the use of bisthiazolidines (BTZs) as a novel scaffold, replicating some features of β -lactam substrates, which can be readily synthesized with high yields, are capable of inhibiting NDM-1 in vitro, and can restore the efficacy of imipenem against pathogenic bacteria expressing NDM-1 in time kill assays. The crystal structure of NDM-1 in complex with the most potent inhibitor reveals details of the inhibitor binding interaction and provides a basis for further improvement of this scaffold.

RESULTS AND DISCUSSION

Inhibition of MBLs present in Gram-negative bacteria is challenging for two main reasons: (1) covalent enzyme–intermediate (EI) adducts do not form during catalysis,^{1,23} and (2) their broad substrate spectrum, which for most MBLs results from a wide, open active site groove containing few (if any) specific sites for substrate recognition. The most critical consideration in the catalytic mechanism is the activation of a Zn(II)-bound water/hydroxide nucleophile and the stabilization, by the Zn(II) ion at the Zn2 site, of an anionic intermediate that forms during hydrolysis of some cephalosporins and carbapenems.^{24–26}

Substrate recognition in MBLs is largely driven by interaction with the metal ions,²⁷ particularly Zn2.²⁸ The β -lactam carboxylate present at position C3' in penicillins and carbapenems and in position C4' in cephalosporins is able to bind Zn2, as well as to interact with a conserved charged residue at position 224, as seen in some of the structurally characterized enzyme–product (EP) or EI complexes.^{11,29,30} Hence, we sought to design an NDM-1 inhibitor scaffold replicating these interactions while at the same time considering other available data related to MBL–substrate interactions.

The rationale for our design of BTZ inhibitors is as follows. We reasoned that bicyclic substrates are well recognized by MBLs. In contrast, monocyclic β -lactam compounds (such as the monobactam antibiotic aztreonam) do not bind productively, because binding through the sulfonate moiety to Zn²⁺ orients the carbonyl group far away from the nucleophile.^{31,32} Second, the tetrahedral bridgehead nitrogen of bicyclic β -lactam antibiotics is important for affinity, because γ -lactam analogues of the penicillins, which have a planar bridgehead nitrogen, are not substrates of the *Bacillus cereus* BcII MBL.³³

On the basis of the substrate structural features outlined above, we envisioned that BTZs could mimic substrate recognition by MBLs (Scheme 1). The motivation is based on the ability of BTZs to (1) mimic a bicyclic β -lactam compound while being devoid of β -lactam functionality, (2) retain the bridging N and the carboxylate able to interact with Zn²⁺, and (3) accommodate additional metal-binding groups targeting the essential Zn center.

The BTZ compounds include a free thiol, which is a high-affinity Zn(II) binding group, as well as a carboxylate, and present these with different relative orientations. The BTZs were synthesized by double condensation of aminothiols and the mercaptoacetaldehyde dimer, as shown in Table 1.³⁴ We prepared four BTZs: L-CS319 and L-VC26 and their enantiomers. The use of penicillamine as a precursor endows these compounds with the C7 *gem*-dimethyl group present in penicillins (Scheme 1). This synthetic strategy allowed us to obtain the targeted compounds with high yields and diastereomeric ratios, starting from the readily available precursors, L- or D-cysteine (Cys) and L- or D-penicillamine (PNA). Unfortunately, attempts to isolate the minor diastereomer (the *anti* compound), failed in both cases for Cys or PNA.

We studied the effect of these BTZs on the initial rates of imipenem hydrolysis by NDM-1. This analysis revealed a competitive inhibition model with inhibition constants (K_i ; Table 2 and Figure S1) ranging between 7 and 19 μ M. In all four cases, the progress curves reflected a single velocity for the onset of inhibition, and we did not observe a curvature of the reaction progress curves over a time scale where the uninhibited reaction progress curve is linear (Figure S2). These observations allowed us to discard time-dependent inhibition and the possibility of a two-state binding process, in contrast to what we have recently reported for inhibition of VIM MBLs by these BTZ compounds.³⁵ The most active compound was L-CS319. The observation that L-CS319 binds with greater affinity than D-CS319 (which features more penicillin-like carboxylate stereochemistry) suggests that thiol binding is the main determinant of inhibition, overriding stereochemical preferences involved in substrate binding. The penicillamine derivatives L- and D-VC26, bearing a *gem*-dimethyl group, were nearly 2 times less active than L-CS319.

To investigate uptake into bacterial cells and to observe in real time whether BTZs inhibited NDM-1 directly, we then tested the ability of these compounds to protect imipenem from the hydrolytic activity of NDM-1 in *E. coli* cells by following imipenem hydrolysis using ¹H NMR.³⁶ Addition of the four BTZs inhibited imipenem hydrolysis by bacterial cells (Table 2 and Figure 2). L-CS319 was the most potent inhibitor in bacteria with an IC₅₀ value of 23 μ M, whereas its enantiomer was 4.7 times less active, a difference within the same order of magnitude as that observed in the in vitro experiments. The main differences between

inhibitory potencies measured in vitro and in bacterial cells were observed for the *gem*-dimethyl compounds, which displayed IC₅₀ values between 180 and 200 μ M, 1 order of magnitude less potent than L-CS319. The relatively high IC₅₀ values for these compounds might arise from differences in cell permeability.

These results encouraged us to broaden our cell-based assays using three NDM-1-producing clinical isolates, *Klebsiella pneumoniae* Ca01.37, *Acinetobacter baumannii* 1.58, and *Providencia rettgeri* Ch01.27. Strikingly, our results showed between 7 and 3 log₁₀-fold reduction of viable cell counts on exposure to sublethal concentrations of imipenem in the presence of the four BTZ inhibitors (Figures 3 and S7). Hence, these findings demonstrate the ability of these inhibitors to restore the activity of imipenem against NDM-1-producing clinical isolates. More noteworthy, because the outer membrane of *Acinetobacter* spp. acts as a substantial barrier against the penetration of antibiotics,^{37,38} our data show that penetration against difficult to treat pathogens is an extremely favorable property of these compounds. Finally, these compounds do not act as direct antimicrobials, as the BTZs independently do not decrease the viable cell number when compared to broth-only controls in in vitro time kill experiments (Figure S7).

MBLs are members of an extensive metalloenzyme superfamily that includes multiple human homologues.³⁹ Candidate MBL inhibitors should therefore show selectivity for MBLs when compared to related human enzymes, as well as lack toxicity against human cells. Thus, we investigated the ability of the most potent inhibitor in vitro (L-CS319) to inhibit human glyoxalase II (hGlx2), an MBL superfamily member involved in oxoaldehyde degradation.⁴⁰ Inhibition of hGlx2 was not observed at concentrations up to 100 μ M L-CS319 (data not shown). To extend this finding, we next tested the cytotoxicity of L-CS319 against cultured mammalian cells. L-CS319 did not show toxic effects against HeLa and Hek 293 cell lines up to a concentration of 500 μ M (Figure S8), indicating a lack of significant inhibitory activity of this compound against other essential human enzymes.

To characterize the mode of inhibition of NDM-1 by L-CS319, we determined a crystal structure of the complex. NDM-1 crystals were obtained in the P1 crystal form (four molecules in the asymmetric unit) described by Feng et al. (pdb 4RM5³⁰) and soaked with 5 mM of inhibitor dissolved in DMSO, yielding a structure for the complex to a resolution of 1.90 Å (above which value completeness in the high-resolution bin rapidly drops). Inspection of difference maps yielded clear evidence for the presence of bound ligand in all four molecules of NDM-1 (Figure S9), although crystallographic *B*-factors varied between individual chains (Table 3). Inhibitor binding has little effect upon the overall structure of NDM-1 (rmsd 0.647 Å between *Ca* atoms using SSMSuperpose⁴¹ compared to PDB accession 3SPU¹⁰). The main differences are in the conformation of the L3 (residues 61–65) and, to a lesser extent, L10 (residues 224–238) loops. Loop L3 is poorly defined in the complex (as evidenced by weaker electron density and elevated crystallographic *B*-factors) and could be modeled in its entirety for only one of the four molecules (Figure S10).

The inhibitor is bound to the NDM-1 active site, which contains two zinc ions bound to the canonical metal ligands of B1MBLs. The sulfur atom of the mercaptomethyl group is positioned nearly equidistant between the two zinc ions, displacing the bridging water/

hydroxide molecule that is proposed to be the attacking nucleophile (Figure 4), but with little impact on the Zn1–Zn2 distance (3.7 vs 3.8 Å in the unbound form). The coordination geometry of the two zinc ions is tetrahedral, in contrast to the structure of unliganded NDM-1, which features a five-coordinated Zn2 ion, indicating that inhibitor binding is able to displace the second “apical” Zn2-bound water molecule that is a feature of many unliganded MBL structures. The carboxylate moiety does not bind Zn2, but instead makes hydrogen bonds with water molecules (Wat; Figure 4) that are themselves connected to Ne of K224.

Crystal structures have been deposited for complexes of NDM-1 with hydrolysis products (EP complexes) generated from a variety of β -lactams^{9,11,30} and with the thiol-containing captopril.¹¹ Comparison of the BTZ complex with these structures (Figure 5) identifies both similarities in the interactions of these different ligands with NDM-1 and some features that are unique to BTZ binding. First, the position of the BTZ thiol, displacing the “bridging” water molecule, is very similar to that occupied by the free thiol of captopril or the carboxylate group of hydrolyzed meropenem, but differs from that of the bridging water present in EP complexes of penicillins or cephalosporins. Second, the Zn1–Zn2 distance resembles that observed in complexes with L-captopril (3.59 Å; pdb 4EXS) and hydrolyzed cefuroxime (3.83 Å; pdb 4RL0) but is considerably shorter than in EP complexes of penicillins and the cephalosporin cephalexin (ca. 4.6 Å) or, to a lesser extent, meropenem (pdb 4EYL; 4.05 Å). Third, the tetrahedral coordination geometry for both Zn1 and Zn2 differs from the 5- and 6-coordination typically observed in EP complexes, but resembles that for the captopril structure. Lastly, the BTZ carboxylate group occupies a unique position, making water-mediated interactions with K224, whereas in all β -lactam EP complexes so far described the equivalent (C2 or C3) carboxylate is positioned to form a bridge between Zn2 and K224. The complex with L-captopril does not feature a Zn2–carboxylate interaction. Hence, as in the case of β -lactam EP adducts of NDM-1, K224 orients the inhibitor for binding to the dinuclear metal site. Mimicking the interaction of β -lactams with the Zn(II) ions and/or K224 may be productive for the development of MBL-specific inhibitors. Finally, the bridging N atom in the BTZ scaffold is far from the zinc ions (at a distance of 5.5 Å from Zn1 and 4.4 Å from Zn2), in contrast to what has been reported in different EP complexes and proposed for EI species. We attribute this difference to the presence of the thiol moiety, which we propose dominates binding to the metal site and, in so, doing limits the extent to which interactions of BTZs with NDM-1 fully mimic those made by β -lactams.

We recently obtained the crystal structure of L-CS319 bound to a related B1MBL, VIM-2, for which BTZ inhibition was described by a slow-binding model (see above). In this work we observed binding of L-CS319 to VIM-2 in two conformations. Binding of L-CS319 to NDM-1 resembles the more populated of these, in which the mercaptomethyl sulfur atom is also positioned between the two zinc ions, and the inhibitor carboxylate is also involved in interactions with the protein main chain. However, in the case of VIM-2, which lacks the conserved K224 found in NDM-1 (and most other subclass B1MBLs), the BTZ carboxylate instead contacts the main-chain carbonyl groups of N233 and (via a water molecule) C221. These interactions are present in both of the observed modes of BTZ binding to VIM-2. We consider it possible that these more plastic interactions involving the BTZ carboxylate

permit multiple modes of binding to VIM-2, resulting in the different mode of inhibition that is observed in solution experiments. Notably, VIM-2 R228, a residue previously proposed to substitute for K224 in many VIM enzymes, is not optimally oriented for H-bonding to the BTZ carboxylate and is present in two conformations, of which the second (conformer B; Figure S11) cannot participate in BTZ binding. This, together with our observation that a leucine substitution at position 228 has little impact upon BTZ affinity, further supports our contention that the BTZ carboxylate occupies a less well-defined binding pocket in VIM-2, compared to NDM-1. We also note that differences in the conformation of the L3 loop (see below) may also serve to shift the position of the BTZ bicyclic ring system in the major conformer of the VIM-2 complex, compared to its location in the present NDM-1 structure (Figure S11).

In addition to hydrogen-bonding and metal coordination interactions, the inhibitor makes hydrophobic contacts with residues M61 and V67 at the base of loop L3 and with W87 of loop L5. Mutagenesis studies on NDM-1 suggest that loop L3 is important in substrate recognition.⁴² Indeed, improvement in IMP-1 inhibition by a series of succinic acid derivatives was achieved by optimizing hydrophobic interactions in the active site.¹⁵ It is notable that the conformation of loop L3 varies in the different NDM-1 structures, with the meropenem EP and cefepime complexes in particular differing from the native structure. Although caution must be exercised in making comparisons as loop L3 is generally less well-defined in NDM-1 structures, has relatively high *B*-factors, and is frequently involved in crystal contacts, we observe that in the BTZ complex loop L3 adopts a more “closed” conformation, overlaying the active site, than is the case for other structures so far reported (Figure 5). Indeed, the distance from the Zn1 (trihistidine) site to the C α of G63 at the apex of the L3 loop varies between 17.9 Å (this structure), 20.1 Å (unliganded enzyme), and the complexes with hydrolyzed ampicillin (21.4 Å), hydrolyzed meropenem (18.4 Å), and L-ceftazidime (19.6 Å). We anticipate that the BTZ scaffold, particularly L-CS319, can be further decorated to improve recognition by hydrophobic moieties located in the L3 and L5 loops. We further note that the conformation of the L10 loop also differs between the native structure, the BTZ and cefepime complexes, and the various β -lactam EP complexes, most likely as a result of contacts between the side chain of N233 and the EP carboxylate groups. Modifying the BTZ scaffold to enable exploitation of similar interactions may offer a further route to improving inhibitor potency.

In summary, we report the successful use of the bithiazolidine scaffold as the basis for new inhibitors of the MBL NDM-1. All compounds efficiently inhibited NDM-1, with one showing low micromolar inhibition both in vitro and in bacterial cells, as well as the ability to restore carbapenem efficacy against NDM-1-producing clinical isolates. Two key elements of this compound are a thiol group that binds by bridging the two Zn(II) ions in the NDM-1 active site and a carboxylate that interacts with K224. The approach outlined herein provides a novel, efficient strategy for MBL inhibition, inspired by key elements of β -lactam binding and hydrolysis, and provides a flexible scaffold for further optimization.

METHODS

Protein Preparation

For kinetic studies, the *bla*_{NDM-1} gene encoding the protein lacking the first 38 residues (including the leader sequence) was cloned between the *Nde*I and *Xho*I restriction sites of a modified version of the pET-28 (+) plasmid in which the thrombin cleavage site was replaced by a TEV cleavage site.^{43,44} The mature NDM-1 (residues 32–294, BBL numbering) was produced in *Escherichia coli* BL21(DE3). The bacterial culture was grown at 37 °C in M9 minimal media until it reached OD₆₀₀ = 0.6. Then, NDM-1 production was induced by addition of 0.5 mM isopropyl β-D-1-thiogalactopyranoside (IPTG). At the time of induction of protein expression, the growth medium was supplemented with 0.5 mM ZnSO₄. Cells were incubated overnight at 18 °C. All subsequent purification steps were performed at 4 °C. The cells were harvested and resuspended in 50 mM Tris-Cl, pH 8.0, 200 mM NaCl and supplemented with 10 μg/mL DNase, 4 mM MgCl₂, 2 mM phenylmethanesulfonyl fluoride (PMSF), and 10 mM β-mercaptoethanol. *E. coli* cells were disrupted by sonication (five cycles of 30 s with 1 min between), and the insoluble material was removed by centrifugation for 60 min at 15000g. The crude extract was loaded onto a Ni-Sepharose column equilibrated with buffer A (50 mM Tris-Cl, pH 8.0, 200 mM NaCl, 10 mM β-mercaptoethanol), the column was washed with 100 mL of buffer A, and His6x-NDM-1 was eluted with buffer B (50 mM Tris-Cl, pH 8.0, 200 mM NaCl, 10 mM β-mercaptoethanol, 500 mM imidazole) using a linear gradient (0–100% buffer B, in 100 mL). Then, 100 μM His6x-NDM-1 was mixed with the TEV protease (1:50 TEV:His6x-NDM-1 ratio), and the mixture was incubated for 16 h at 4 °C during dialysis against 100 volumes of 50 mM Tris-Cl, pH 8.0, 200 mM NaCl, 10 mM β-mercaptoethanol. NDM-1 was then loaded onto a Ni-Sepharose column to separate it from the His6x tag, the uncleaved fusion protein, and the His6x-tagged TEV protease. NDM-1 was collected in the flow-through of the column with a purity >95%, as determined by SDS-PAGE. β-Mercaptoethanol was removed from the protein sample by one 12-h dialysis step of 100 μM NDM-1 against 100 volumes of 10 mM HEPES, pH 7.5, 200 mM NaCl, 200 μM ZnSO₄, followed by three 4-h dialysis steps against 100 volumes of 10 mM HEPES, pH 7.5, 200 mM NaCl. NDM-1 was concentrated using Centricon ultrafiltration devices (Millipore, Bedford, MA, USA) to a final concentration of 200 μM. Protein concentrations were determined from the absorbance at 280 nm using a molar absorption coefficient⁴⁵ (ϵ_{280}) of 28500 M⁻¹ cm⁻¹. The average protein yield was 50 mg/L culture. For X-ray crystallography, NDM-1 lacking the first 26 amino acids (including the leader sequence) was expressed from the pOPINF T7 vector.⁴⁶ Recombinant NDM-1 was expressed and purified according to the method of Rydzik et al.⁴⁷ and concentrated to 35 mg/mL by ultrafiltration.

Representative Synthesis of Bisthiazolidines.⁴⁸

Synthesis of (2R,5S,8R)-8-Carboxylate-2-mercaptomethyl-1-aza-3,6-dithiobicyclo[3.3.0]octane (L-CS319)—1,4-Dithiane-2,5-di-thiol (0.8 g, 5.0 mmol) and *p*-TsOH ac. (0.030 g, 0.17 mmol) were added to a stirred suspension of L-cysteine (0.5 g, 4.1 mmol) in ethanol (16 mL). The mixture was heated at reflux for 2 h. It was then cooled and poured into brine, extracted with CH₂Cl₂ (5 × 30 mL), dried (Na₂SO₄), and filtered, and the solvent was removed under reduced pressure. The residue was purified by chromatography

on SiO₂ (1:3:0.1 EtOAc/hexane/AcOH) to give compound L-CS319 (0.830 g, 86%, *syn/anti* 95:05) as a white solid: mp 103–104 °C; ¹H NMR (CDCl₃) δ 1.86 (t, *J* = 8.5 Hz, 1H_{SH}), 2.81 (dd, *J* = 8.5, 6.9 Hz, 2H), 3.11 (dd, *J* = 12.0, 4.2 Hz, 1H), 3.33 (dd, *J* = 11.4, 7.1 Hz, 1H), 3.43 (dd, *J* = 11.4, 3.3 Hz, 1H), 3.55 (dd, *J* = 12.0, 5.8 Hz, 1H), 4.25 (dd, *J* = 7.1, 3.3 Hz, 1H), 4.32 (t, *J* = 6.9 Hz, 1H), 5.05 (dd, *J* = 5.8, 4.2 Hz, 1H); ¹³C NMR ((CD₃)₂CO) δ 34.0, 34.3, 39.2, 71.5, 74.5, 75.6, 172.1; HRMS calculated for C₇H₁₁NO₂S₃, [M + H]⁺ 238.0025, found 238.0033; [α]_D = −57.7° (20 °C, AcCN, *c* 0.6).

Synthesis of (2S,5R,8S)-8-Carboxylate-2-mercaptomethyl-1-aza-3,6-dithiobicyclo[3.3.0]octane (D-CS319)—An analogous route to the one described for L-CS319, starting from D-cysteine, was used. The spectroscopic properties were identical to those obtained for L-CS319, [α]_D = +63.1° (20 °C, AcCN, *c* 0.6).

Synthesis of (2R,5S,8R)-2-Mercaptomethyl-7-dimethyl-8-carboxylate-1-aza-3,6-dithiobicyclo[3.3.0]octane (L-VC26)—An analogous route to the one described for L-CS319, starting from L-penicillamine, was used. Purification by chromatography on SiO₂ (1:3, EtOAc/hexane) gave compound L-VC26 (89%, *syn/anti* 95:0.5): ¹H NMR (CDCl₃) δ 1.52 (s, 3H), 1.62 (s, 3H), 1.89 (t, *J* = 8.7 Hz, 1H_{SH}), 2.81 (m, 2H), 3.06 (dd, *J* = 11.7, 5.4 Hz, 1H), 3.43 (dd, *J* = 11.7, 6.6 Hz, 1H), 3.80 (s, 1H), 4.31 (t, *J* = 7.3 Hz, 1H), 4.98 (dd, *J* = 6.6, 5.4 Hz, 1H); ¹³C NMR (CDCl₃) δ 28.0, 28.1, 32.0, 40.5, 55.1, 68.7, 75.7, 78.5, 170.4; HRMS calculated for C₉H₁₆NO₂S₃, [M + H]⁺ 266.0343, found 266.0330; [α]_D = −45.2° (20 °C, MeOH, *c* 1.0).

Synthesis of (2S,5R,8S)-2-Mercaptomethyl-7-dimethyl-8-carboxylate-1-aza-3,6-dithiobicyclo[3.3.0]octane (D-VC26)—It was prepared following an analogous route to the one described for L-CS319, starting from D-penicillamine. The spectroscopic properties were identical to those obtained for L-VC26; [α]_D = +40.0° (20 °C, MeOH, *c* 1.0).

Inhibition Assays on NDM-1

Hydrolysis of imipenem by NDM-1 was monitored using a Jasco V-670 spectrophotometer by following the changes in absorbance at 300 nm using a $\epsilon_{300} = -9000 \text{ M}^{-1} \text{ cm}^{-1}$. The reaction medium employed was 10 mM HEPES, pH 7.5, 200 mM NaCl, 50 $\mu\text{g/mL}$ BSA, and 20 μM ZnSO₄ at 30 °C. Reactions were carried out in 0.1 cm path length quartz cuvettes in a final volume of 300 μL , with a final enzyme concentration of 1 nM. Bisthiazolidines were dissolved in DMSO to a final concentration of 100 mM and then diluted 10-fold (to 10 mM) in 10 mM HEPES, pH 7.5, 200 mM NaCl. Appropriate volumes of the 10 mM stock solutions were used to achieve the desired final concentrations. The final DMSO concentration in the reaction mixture was then maintained between 0.01 and 0.07%, which did not alter the enzyme activity (data not shown). The assay was initiated by the addition of NDM-1 to the mixture of substrate and inhibitor. In the presence of inhibitor, the initial phase of the time courses was linear but showed a decreased rate of hydrolysis with respect to the reaction in the absence of inhibitor. The initial rate of reaction for each substrate or substrate–inhibitor concentration, under steady state conditions (<5% of substrate consumed), was calculated from the slope of the initial linear phase of the respective time course. Inhibition constants (*K_i*) were evaluated by nonlinear fitting of the initial velocities

at various concentrations of the substrates and inhibitors, with the equations for different inhibition models as implemented in GraphPad 5.0. Best fits were obtained with the competitive inhibition model using the equation $v_0 = ((v_{\max} \times [S]) / (K_M \times (1 + [I]/K_i) + [S]))$ (Figure S1). The inhibition constants (K_i) are shown with their corresponding standard errors obtained from the fit (Table 2). We obtained the Lineweaver–Burk plots for each bisthiazolidine from the fits to the competitive inhibition model using the equation $(1/v_0) = (1/v_{\max}) \times ((1/[S]) \times K_M \times (1 + ([I]/K_i)) + 1)$ (Figure S3). The bisthiazolidine inhibitors did not show a significant absorption spectrum, allowing us to discard possible interferences with the measurements (Figure S18).

Glyoxalase Activity Measurements

The inhibition analyses for hydroxyacylglutathione hydrolase, human glyoxylase II (hHAGH), were performed following the hHAGH assay from R&D Systems. The hHAGH assay was carried out using a BMG Labtech Pherastar FS microplate reader using UV-Star 96 well plates (Greiner Bio-One). L-CS319 was screened at a single concentration (100 μ M) in triplicate. The inhibitor was incubated for 10 min with the enzyme prior to addition of the substrate. The rate of hydrolysis of *S*-lactoylglutathione (0.5 mM, supplemented with DTNB (200 μ M) to form a substrate mixture) by recombinant hHAGH (0.2 ng/ μ L) was monitored at 405 nm in the presence of L-CS319. EDTA was used as control. No inhibition was detected at these assay conditions.

E. coli Cell Preparations for Inhibition Studies

We constructed a plasmid for the periplasmic expression of NDM-1 (pMBLeNDM-1), in which the *bla*_{NDM-1} gene is under the control of the pLac promoter (Scheme S1). *E. coli* cells carrying the pMBLe vector (without the *bla*_{NDM-1} gene) or the pMBLeNDM-1 vector were inoculated into 10 mL of lysogeny broth (LB) medium in the presence of 25 μ g/mL gentamicin and were grown with shaking (220 rpm) at 37 °C until cells reached OD₆₀₀ = 0.6. At that time, 100 μ M IPTG was added for NDM-1 β -lactamase induction, and cells were grown for 2 h at 37 °C with shaking (220 rpm). Cell cultures were centrifuged at 1000g for 4 min at 4 °C, the supernatant was discarded, and the cell pellets were washed thoroughly by resuspending them in 1 mL of buffer (50 mM sodium phosphate, pH 7.0) and were then pelleted again by centrifugation (1000g, for 4 min at 4 °C). This process was repeated three times, and finally cells were resuspended in buffer to OD₆₀₀ = 0.1 for NMR studies. Lastly, 500 μ L of final cell suspensions (in 50 mM sodium phosphate, pH 7.0, at 90% H₂O/10% D₂O) was placed in the NMR tube for data acquisition. Different concentrations of each compound and/or 500 μ M of imipenem were added for estimation of the IC₅₀ values. Supernatants from the cell suspensions were collected by centrifugation (1000g for 10 min at 4 °C) and then filtered through 0.22 μ m filters.

Plating Colony Tests for NDM-1-Bearing *E. coli* Cells

We obtained serial 10³, 10⁴, 10⁵, 10⁶, 10⁷, and 10⁸-fold dilutions from stock suspensions of NDM-1-bearing *E. coli* cells. Then, we inoculated an LB-agar plate containing 25 μ g/mL gentamicin with 10 μ L drops of each dilution. The drops were allowed to dry on the plate, and the plate was incubated at 37°C overnight.

¹H NMR Measurements and Analyses

All spectra were acquired on a Bruker Avance 600 MHz spectrometer equipped with a TXI probe. We used a sweep width of 10204 Hz for 1D ¹H NMR experiments. All spectra were acquired with 64 scans, and the temperature was kept constant at 25 °C. Water suppression was achieved by means of the excitation sculpting scheme; the water-selective 180 °C sine-shaped pulse was 2 ms long. The FID was collected in 32K data points. A 1 Hz exponential line broadening function was applied prior to Fourier transformation. NMR spectra were processed and analyzed with TopSpin 3.0. All spectra in a given series were plotted at the same scaling ratio.

Whole-Cell IC₅₀ Measurements and Analyses

We confirmed that imipenem is sufficiently stable in buffer or in the presence of *E. coli* cells lacking carbapenemases (Figure S4). However, when a 500 μM imipenem solution was exposed to a suspension of *E. coli* cells expressing NDM-1, the carbapenem was degraded within 9–15 min (Figure 2). Cell lysis leading to NDM-1 leakage into the medium was not observed, confirming that the reaction occurred within the bacterial periplasm (Figure S5). Cell viability after 1 h of incubation during the NMR measurements was verified (Figure S6).

We then performed the IC₅₀ measurements according to the procedure of Dalvit and co-workers.⁴⁹ To evaluate the potency of the inhibitors we calculated the percentage of the inhibition seen 15 min after the initiation of the reaction using eq 1

$$\%inhibition = 100 \times [1 - ([S_{TOT}] - [S_w]) / ([S_{TOTAL}] - [S_{w/o}])] \quad (1)$$

where [S_w] and [S_{w/o}] are given by the integrals of the substrate signals (between 1.21 and 1.18 ppm of imipenem in this case) in the presence and absence of inhibitor, respectively. [S_{TOTAL}] is the sum of [S_{w/o}] and [P_{w/o}] or [S_w] and [P_w], where [P_w] and [P_{w/o}] are the integrals of the product signals (between 1.17 and 1.12 ppm of hydrolyzed imipenem in this case) in the presence and absence of the inhibitor, respectively. IC₅₀ values can be obtained by fitting the data of percent inhibition versus inhibitor concentration to eq 2

$$\%inhibition = 100 \times [1 - 1 / (1 + ([I] / IC_{50})^n)] \quad (2)$$

where [I] is the concentration of the inhibitor and *n* is the cooperativity factor. The IC₅₀ values are presented with the corresponding standard errors obtained from the fit (Table 2).

Crystallization and Structure Determination

We used a version of NDM-1 lacking the first 26 amino acids at a concentration of 35 mg/mL. Crystals were obtained from 100 mM MES, pH 6.5, 25% (w/v) PEG 2000 monomethyl ether and soaked for 10 min in a solution of mother liquor containing 5 mM of the bithiazolidine L-CS319 and 5% dimethyl sulfoxide (DMSO), before transient transfer

to mother liquor supplemented with 25% glycerol and snap-freezing in liquid nitrogen. X-ray diffraction data were collected on a Pilatus M2 detector mounted on beamline I04-1 of the Diamond Light Source synchrotron radiation facility (Didcot, UK). Data were integrated using the program XDS⁵⁰ with space group assignment by POINTLESS⁵¹ as implemented in the XIA2 crystallography pipeline,⁵² and scaled and merged using SCALA⁵³ as part of the CCP4 crystallography suite.⁵⁴ The structure was solved by molecular replacement using PHASER⁵⁵ with unliganded NDM-1 (pdb 3SPU)¹⁰ as a search model. The model was rebuilt using Coot⁵⁶ and refined using PHENIX.⁵⁷ The quality of the final structure was assessed with MolProbity.⁵⁸

Cytotoxicity Assays

HeLa/HEK 293 cells were seeded (5000 or 2000 per well, respectively) in normal DMEM using 96-well plates. After 24 h, the wells were closed and supplemented with the inhibitor (final DMSO concentration - 1%). Following a further 24 h incubation period, 20 μ L of tetrazolium (MTS, CellTiter96Aqueous One Solution (Promega)) was added to the medium in each well. The plate was incubated at 37 °C with 5% CO₂ for 4 h in the dark before the absorbance was read at 495 nm to determine cell proliferation values.

In Vitro Time Kill Study

Three clinical strains expressing NDM-1 as the only MBL were employed for these experiments (Table S1).⁵⁹ NDM-1-producing *Klebsiella pneumoniae* (imipenem MIC = 8 mg/L), *Providencia rettgeri* (imipenem MIC = 64 mg/L),⁵⁹ and *Acinetobacter baumannii* (imipenem MIC = 128 mg/L) were cultured overnight at 37 °C in Muller Hinton broth (MHB) supplemented with 50 mg/L ampicillin. The following day, 1.5 μ L of the overnight cultures was inoculated in 1 mL of MHB to obtain a bacterial suspension of approximately 10⁶ CFU/mL. To examine the effects of the novel bithiazolidine compounds on bacterial growth, the bacterial suspensions were grown at 37 °C under different conditions: MHB alone (growth control) or supplemented with 0.4% DMSO (growth control), sublethal concentrations of imipenem (4 mg/L for *K. pneumoniae* and 16 mg/L for *A. baumannii* and *P. rettgeri*), 100 mg/L of each inhibitor, or a combination of imipenem and inhibitor. Samples (10 μ L) were removed at time intervals of 100, 300, and 500 min of exposure, and serial dilutions were performed on MHB. The number of viable cells was determined by spotting 20 μ L of each dilution on Muller Hinton agar (MHA). The plates were incubated at 37°C overnight, and the numbers of colonies were counted. Results shown are the mean of three biological replicates.

The inhibitors do not have any antimicrobial effect on their own, as differences could not be detected in viable cell number between inhibitor-exposed cells and broth-only controls (Figure S7).

Supplementary Material

Refer to Web version on PubMed Central for supplementary material.

Acknowledgments

This work was supported by funds and/or facilities provided by the Cleveland Department of Veterans Affairs, the Department of Veterans Affairs Merit Review Program, the Veterans Integrated Service Network 10 Geriatric Research, Education, and Clinical Center (VISN 10 GRECC), ANPCyT grants to A.J.V., and the National Institute of Allergy and Infectious Diseases of the National Institutes of Health under Awards 5R01AI100560-03, R01 AI100560, and R01 AI063517. A.J.V. and L.I.L. are CONICET staff members. M.M.G. thanks CONICET for fellowships. V.C. is grateful for a fellowship from ANII (POS_X_2014). J.S., J.B., and C.J.S. acknowledge funding from the U.K. Medical Research Council (UK–Canada Team Grant G1100135). We thank Diamond Light Source for access to beamline I04-1 (Proposal MX313) that contributed to the results presented here.

References

1. Fisher JF, Meroueh SO, Mobashery S. Bacterial resistance to β -lactam antibiotics: compelling opportunism, compelling opportunity. *Chem Rev.* 2005; 105:395–424. [PubMed: 15700950]
2. van Duin D, Kaye KS, Neuner EA, Bonomo RA. Carbapenem-resistant Enterobacteriaceae: a review of treatment and outcomes. *Diagn Microbiol Infect Dis.* 2013; 75:115–120. [PubMed: 23290507]
3. Bush K. Alarming β -lactamase-mediated resistance in multidrug-resistant Enterobacteriaceae. *Curr Opin Microbiol.* 2010; 13:558–564. [PubMed: 20920882]
4. Patel G, Bonomo RA. Status report on carbapenemases: challenges and prospects. *Expert Rev Anti-Infect Ther.* 2011; 9:555–570.
5. Munoz-Price LS, Poirel L, Bonomo RA, Schwaber MJ, Daikos GL, Cormican M, Cornaglia G, Garau J, Gniadkowski M, Hayden MK, Kumarasamy K, Livermore DM, Maya JJ, Nordmann P, Patel JB, Paterson DL, Pitout J, Villegas MV, Wang H, Woodford N, Quinn JP. Clinical epidemiology of the global expansion of *Klebsiella pneumoniae* carbapenemases. *Lancet Infect Dis.* 2013; 13:785–796. [PubMed: 23969216]
6. Kumarasamy KK, Toleman MA, Walsh TR, Bagaria J, Butt F, Balakrishnan R, Chaudhary U, Doumith M, Giske CG, Irfan S, Krishnan P, Kumar AV, Maharjan S, Mushtaq S, Noorie T, Paterson DL, Pearson A, Perry C, Pike R, Rao B, Ray U, Sarma JB, Sharma M, Sheridan E, Thirunarayan MA, Turton J, Upadhyay S, Warner M, Welfare W, Livermore DM, Woodford N. Emergence of a new antibiotic resistance mechanism in India, Pakistan, and the UK: a molecular, biological, and epidemiological study. *Lancet Infect Dis.* 2010; 10:597–602. [PubMed: 20705517]
7. Walsh TR, Weeks J, Livermore DM, Toleman MA. Dissemination of NDM-1 positive bacteria in the New Delhi environment and its implications for human health: an environmental point prevalence study. *Lancet Infect Dis.* 2011; 11:355–362. [PubMed: 21478057]
8. Yong D, Toleman MA, Giske CG, Cho HS, Sundman K, Lee K, Walsh TR. Characterization of a new metallo- β -lactamase gene, bla(NDM-1), and a novel erythromycin esterase gene carried on a unique genetic structure in *Klebsiella pneumoniae* sequence type 14 from India. *Antimicrob Agents Chemother.* 2009; 53:5046–5054. [PubMed: 19770275]
9. Zhang H, Hao Q. Crystal structure of NDM-1 reveals a common β -lactam hydrolysis mechanism. *FASEB J.* 2011; 25:2574–2582. [PubMed: 21507902]
10. King D, Strynadka N. Crystal structure of New Delhi metallo- β -lactamase reveals molecular basis for antibiotic resistance. *Protein Sci.* 2011; 20:1484–1491. [PubMed: 21774017]
11. King DT, Worrall LJ, Gruninger RJ, Strynadka NCJ. New Delhi metallo- β -lactamase: structural insights into β -lactam recognition and inhibition. *J Am Chem Soc.* 2012; 134:11362–11365. [PubMed: 22713171]
12. Galleni M, Lamotte-Brasseur J, Rossolini GM, Spencer J, Dideberg O, Frère JM. Standard numbering scheme for class B β -lactamases. *Antimicrob Agents Chemother.* 2001; 45:660–663. [PubMed: 11181339]
13. Liénard BMR, Hüting R, Lassaux P, Galleni M, Frère JM, Schofield CJ. Dynamic combinatorial mass spectrometry leads to metallo- β -lactamase inhibitors. *J Med Chem.* 2008; 51:684–688. [PubMed: 18205296]

14. Mollard C, Moali C, Papamichael C, Damblon C, Vessilier S, Amicosante G, Schofield CJ, Galleni M, Frère JM, Roberts GC. Thiomandelic acid, a broad spectrum inhibitor of zinc beta-lactamases: kinetic and spectroscopic studies. *J Biol Chem.* 2001; 276:45015–45023. [PubMed: 11564740]
15. Toney JH, Hammond GG, Fitzgerald PM, Sharma N, Balkovec JM, Rouen GP, Olson SH, Hammond ML, Greenlee ML, Gao YD. Succinic acids as potent inhibitors of plasmid-borne IMP-1 metallo- β -lactamase. *J Biol Chem.* 2001; 276:31913–31918. [PubMed: 11390410]
16. García-Saez I, Hopkins J, Papamichael C, Franceschini N, Amicosante G, Rossolini GM, Galleni M, Frère JM, Dideberg O. The 1.5-Å structure of *Chryseobacterium meningosepticum* zinc β -lactamase in complex with the inhibitor, D-captopril. *J Biol Chem.* 2003; 278:23868–23873. [PubMed: 12684522]
17. Guo Y, Wang J, Niu G, Shui W, Sun Y, Zhou H, Zhang Y, Yang C, Lou Z, Rao Z. A structural view of the antibiotic degradation enzyme NDM-1 from a superbug. *Protein Cell.* 2011; 2:384–394. [PubMed: 21637961]
18. Zhang YL, Yang KW, Zhou YJ, LaCuran AE, Oelschlaeger P, Crowder MW. Diaryl-substituted azolythioacetamides: Inhibitor discovery of New Delhi metallo- β -lactamase-1 (NDM-1). *ChemMedChem.* 2014; 9:2445–2448. [PubMed: 25048031]
19. Klingler FM, Wichelhaus TA, Frank D, Bernal JC, El-Delik J, Muller HF, Sjuts H, Gottig S, Koenigs A, Pos KM, Pogoryelov D, Proschak E. Approved drugs containing thiols as inhibitors of metallo- β -lactamases: a strategy to combat multidrug-resistant bacteria. *J Med Chem.* 2015; 58:3626–3630. [PubMed: 25815530]
20. Livermore DM, Mushtaq S, Morinaka A, Ida T, Maebashi K, Hope R. Activity of carbapenems with ME1071 (disodium 2,3-diethylmaleate) against Enterobacteriaceae and *Acinetobacter* spp. with carbapenemases, including NDM enzymes. *J Antimicrob Chemother.* 2013; 68:153–158. [PubMed: 22945917]
21. Brem J, van Berkel SS, Aik W, Rydzik AM, Avison MB, Pettinati I, Umland KD, Kawamura A, Spencer J, Claridge TD, McDonough MA, Schofield CJ. Rhodanine hydrolysis leads to potent thioenolate mediated metallo- β -lactamase inhibition. *Nat Chem.* 2014; 6:1084–1090. [PubMed: 25411887]
22. King AM, Reid-Yu SA, Wang W, King DT, De Pascale G, Strynadka NC, Walsh TR, Coombes BK, Wright GD. Aspergillomarasmine A overcomes metallo- β -lactamase antibiotic resistance. *Nature.* 2014; 510:503–506. [PubMed: 24965651]
23. Crowder MW, Spencer J, Vila AJ. Metallo- β -lactamases: novel weaponry for antibiotic resistance in bacteria. *Acc Chem Res.* 2006; 39:721–728. [PubMed: 17042472]
24. Yang H, Aitha M, Hetrick AM, Richmond TK, Tierney DL, Crowder MW. Mechanistic and spectroscopic studies of metallo- β -lactamase NDM-1. *Biochemistry.* 2012; 51:3839–3847. [PubMed: 22482529]
25. Tioni MF, Llarrull LI, Poeylout-Palena AA, Martí MA, Saggu M, Periyannan GR, Mata EG, Bennett B, Murgida DH, Vila AJ. Trapping and characterization of a reaction intermediate in carbapenem hydrolysis by *B. cereus* metallo-beta-lactamase. *J Am Chem Soc.* 2008; 130:15852–15863. [PubMed: 18980308]
26. Wang Z, Fast W, Benkovic SJ. On the mechanism of the metallo-beta-lactamase from *Bacteroides fragilis*. *Biochemistry.* 1999; 38:10013–10023. [PubMed: 10433708]
27. Rasia RM, Vila AJ. Structural determinants of substrate binding to *Bacillus cereus* metallo- β -lactamase. *J Biol Chem.* 2004; 279:26046–26051. [PubMed: 15140877]
28. Meini MR, González LJ, Vila AJ. Antibiotic resistance in Zn(II)-deficient environments: metallo- β -lactamase activation in the periplasm. *Future Microbiol.* 2013; 8:947–979. [PubMed: 23902139]
29. Garau G, Bebrone C, Anne C, Galleni M, Frère JM, Dideberg O. A metallo- β -lactamase enzyme in action: crystal structures of the monozinc carbapenemase CphA and its complex with biapenem. *J Mol Biol.* 2005; 345:785–795. [PubMed: 15588826]
30. Feng H, Ding J, Zhu D, Liu X, Xu X, Zhang Y, Zang S, Wang DC, Liu W. Structural and mechanistic insights into NDM-1 catalyzed hydrolysis of cephalosporins. *J Am Chem Soc.* 2014; 136:14694–14697. [PubMed: 25268575]

31. Poeylout-Palena AA, Tomatis PE, Karsisiotis AI, Damblon C, Mata EG, Vila AJ. A minimalistic approach to identify substrate binding features in B1Metallo- β -lactamases. *Bioorg Med Chem Lett*. 2007; 17:5171–5174. [PubMed: 17644332]
32. Tripathi R, Nair NN. Mechanism of meropenem hydrolysis by New Delhi metallo β -lactamase. *ACS Catal*. 2015; 5:2577–2586.
33. Baldwin JE, Lynch GP, Pitlik J. γ -Lactam analogues of β -lactam antibiotics. *J Antibiot*. 1991; 44:1–24. [PubMed: 2001979]
34. Saiz C, Pizzo C, Manta E, Wipf P, Mahler SG. Microwave assisted tandem reactions for the synthesis of 2-hydrazolyl-4-thiazolidinones. *Tetrahedron Lett*. 2009; 50:901–904. [PubMed: 19756224]
35. Mojica MF, Mahler SG, Bethel CR, Taracila MA, Kosmopoulou M, Papp-Wallace KM, Llarrull LI, Wilson BM, Marshall SH, Wallace CJ, Villegas MV, Harris ME, Vila AJ, Spencer J, Bonomo RA. Exploring the role of residue 228 in substrate and inhibitor recognition by VIM metallo- β -lactamases. *Biochemistry*. 2015; 54:3183–3196. [PubMed: 25915520]
36. Ma J, McLeod S, MacCormack K, Sriram S, Gao N, Breeze AL, Hu J. Real-time monitoring of New Delhi metallo- β -lactamase activity in living bacterial cells by 1H NMR spectroscopy. *Angew Chem, Int Ed*. 2014; 53:2130–2133.
37. Sato K, Nakae T. Outer membrane permeability of *Acinetobacter calcoaceticus* and its implication in antibiotic resistance. *J Antimicrob Chemother*. 1991; 28:35–45.
38. Perez F, Hujer AM, Hujer KM, Decker BK, Rather PN, Bonomo RA. Global challenge of multidrug-resistant *Acinetobacter baumannii*. *Antimicrob Agents Chemother*. 2007; 51:3471–3484. [PubMed: 17646423]
39. Bebrone C. Metallo-beta-lactamases (classification, activity, genetic organization, structure, zinc coordination) and their superfamily. *Biochem Pharmacol*. 2007; 74:1686–1701. [PubMed: 17597585]
40. Sousa Silva M, Gomes RA, Ferreira AE, Ponces Freire A, Cordeiro C. The glyoxalase pathway: the first hundred years... and beyond. *Biochem J*. 2013; 453:1–15. [PubMed: 23763312]
41. Krissinel E, Henrick K. Secondary-structure matching (SSM), a new tool for fast protein structure alignment in three dimensions. *Acta Crystallogr, Sect D: Biol Crystallogr*. 2004; 60:2256–2268. [PubMed: 15572779]
42. Chiou J, Leung TY, Chen S. Molecular mechanisms of substrate recognition and specificity of New Delhi metallo- β -lactamase. *Antimicrob Agents Chemother*. 2014; 58:5372–5378. [PubMed: 24982075]
43. Houben K, Marion D, Tarbouriech N, Ruigrok RWH, Blanchard L. Interaction of the C-terminal domains of sendai virus N and P proteins: comparison of polymerase-nucleocapsid interactions within the paramyxovirus family. *J Virol*. 2007; 81:6807–6816. [PubMed: 17459940]
44. Kapust RB, Tözsér J, Fox JD, Anderson DE, Cherry S, Copeland TD, Waugh DS. Tobacco etch virus protease: mechanism of autolysis and rational design of stable mutants with wild-type catalytic proficiency. *Protein Eng, Des Sel*. 2001; 14:993–1000.
45. Kim Y, Tesar C, Mire J, Jedrzejczak R, Binkowski A, Babnigg G, Sacchettini J, Joachimiak A. Structure of apo- and monometalated forms of NDM-1 – a highly potent carbapenem-hydrolyzing metallo- β -lactamase. *PLoS One*. 2011; 6:e24621. [PubMed: 21931780]
46. Berrow NS, Alderton D, Sainsbury S, Nettleship J, Assenberg R, Rahman N, Stuart DI, Owens RJ. A versatile ligation-independent cloning method suitable for high-throughput expression screening applications. *Nucleic Acids Res*. 2007; 35:e45. [PubMed: 17317681]
47. Rydzik AM, Brem J, van Berkel SS, Pfeffer I, Makena A, Claridge TDW, Schofield CJ. Monitoring conformational changes in the NDM-1 metallo- β -lactamase by 19F NMR spectroscopy. *Angew Chem, Int Ed*. 2014; 53:3129–3133.
48. Saiz C, Castillo V, Fontán P, Bonilla M, Salinas G, Rodríguez-Haralambides A, Mahler SG. Discovering *Echinococcus granulosus* thioredoxin glutathione reductase inhibitors through site-specific dynamic combinatorial chemistry. *Mol Diversity*. 2014; 18:1–12.
49. Dalvit C, Ardini E, Fogliatto GP, Mongelli N, Veronesi M. Reliable high-throughput functional screening with 3-FABS. *Drug Discovery Today*. 2004; 9:595–602. [PubMed: 15239978]

50. Kabsch W. Integration, scaling, space-group assignment and post-refinement. *Acta Crystallogr, Sect D: Biol Crystallogr*. 2010; 66:133–144. [PubMed: 20124693]
51. Evans PR. An introduction to data reduction: space-group determination, scaling and intensity statistics. *Acta Crystallogr, Sect D: Biol Crystallogr*. 2011; 67:282–292. [PubMed: 21460446]
52. Winter G, Dökel S, Jones AK, Scheerer P, Krauss N, Höhne W, Friedrich B. Crystallization and preliminary X-ray crystallographic analysis of the [NiFe]-hydrogenase maturation factor HypF1 from *Ralstonia eutropha* H16. *Acta Crystallogr, Sect F: Struct Biol Cryst Commun*. 2010; 66:452–455.
53. Evans P. Scaling and assessment of data quality. *Acta Crystallogr, Sect D: Biol Crystallogr*. 2006; 62:72–82. [PubMed: 16369096]
54. Winn MD, Ballard CC, Cowtan KD, Dodson EJ, Emsley P, Evans PR, Keegan RM, Krissinel EB, Leslie AGW, McCoy A, McNicholas SJ, Murshudov GN, Pannu NS, Potterton EA, Powell HR, Read RJ, Vagin A, Wilson KS. Overview of the CCP4 suite and current developments. *Acta Crystallogr, Sect D: Biol Crystallogr*. 2011; 67:235–242. [PubMed: 21460441]
55. McCoy AJ, Grosse-Kunstleve RW, Adams PD, Winn MD, Storoni LC, Read RJ. Phaser crystallographic software. *J Appl Crystallogr*. 2007; 40:658–674. [PubMed: 19461840]
56. Emsley P, Lohkamp B, Scott WG, Cowtan K. Features and development of Coot. *Acta Crystallogr, Sect D: Biol Crystallogr*. 2010; 66:486–501. [PubMed: 20383002]
57. Afonine PV, Grosse-Kunstleve RW, Echols N, Headd JJ, Moriarty NW, Mustyakimov M, Terwilliger TC, Urzhumtsev A, Zwart PH, Adams PD. Towards automated crystallographic structure refinement with phenix.refine. *Acta Crystallogr, Sect D: Biol Crystallogr*. 2012; 68:352–367. [PubMed: 22505256]
58. Chen VB, Arendall WB, Headd JJ, Keedy DA, Immormino RM, Kapral GJ, Murray LW, Richardson JS, Richardson DC. MolProbity: all-atom structure validation for macromolecular crystallography. *Acta Crystallogr, Sect D: Biol Crystallogr*. 2010; 66:12–21. [PubMed: 20057044]
59. Lascols C, Hackel M, Marshall SH, Hujer AM, Bouchillon S, Badal R, Hoban D, Bonomo RA. Increasing prevalence and dissemination of NDM-1 metallo- β -lactamase in India: data from the SMART study (2009). *J Antimicrob Chemother*. 2011; 66:1992–1997. [PubMed: 21676902]

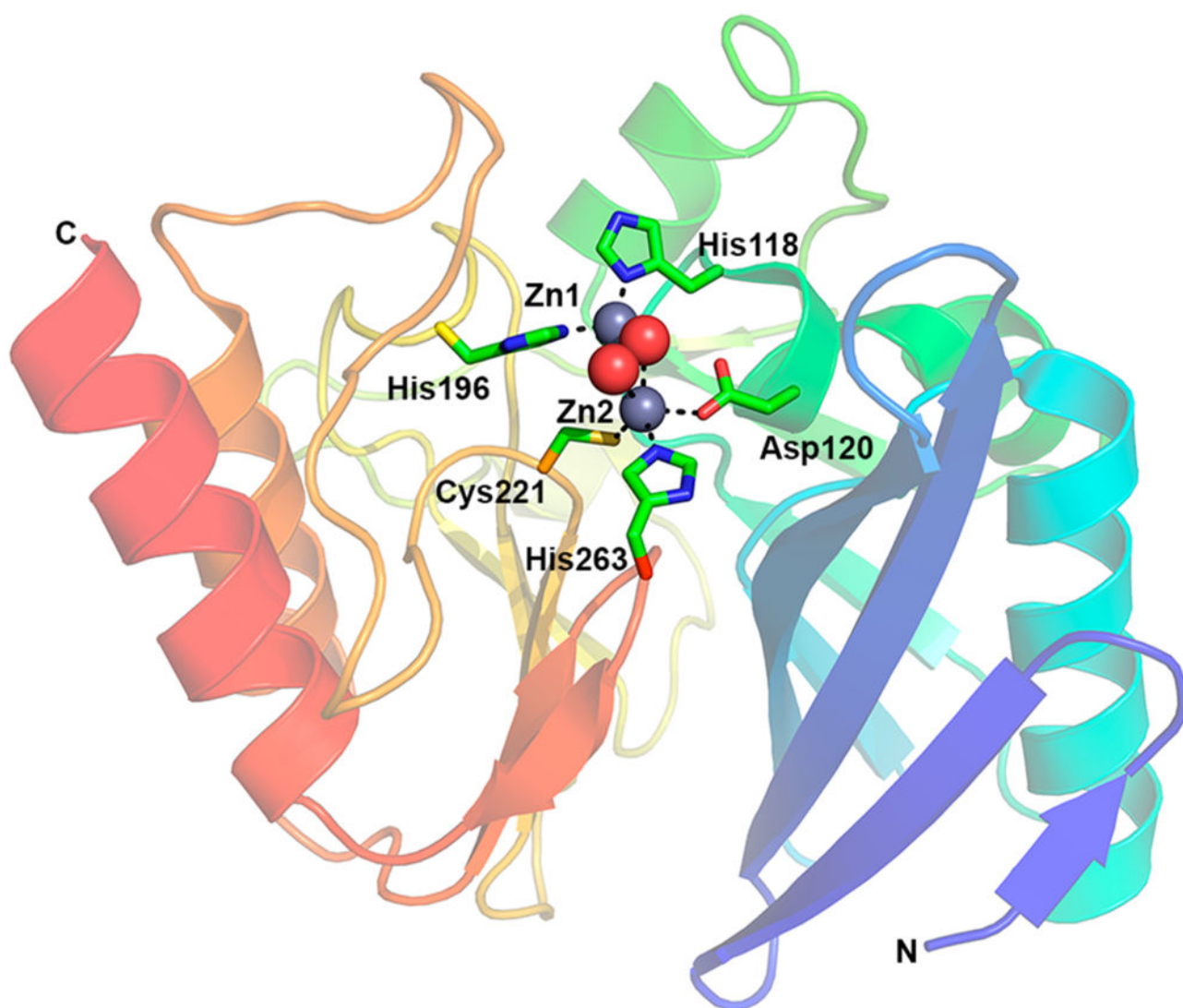


Figure 1.

Structure of NDM-1 (PDB code 3SPU). The enzyme contains a dinuclear metal center in the active site, comprising two Zn(II) ions: one with a tetrahedral coordination sphere (Zn1, coordinated to residues His116, His118, and His196 and a water/ hydroxide molecule) and one in a trigonal bipyramidal coordination sphere (Zn2, coordinated to residues Asp120, Cys221, and His263, a water molecule, and the water/hydroxide molecule). Zinc ions and water molecules are represented as gray and red spheres, respectively. The amino acid side chains are colored according to atom type. The protein main chain is color-ramped from the N-terminus (blue) to the C-terminus (red). This figure was generated using PyMol (www.pymol.org).

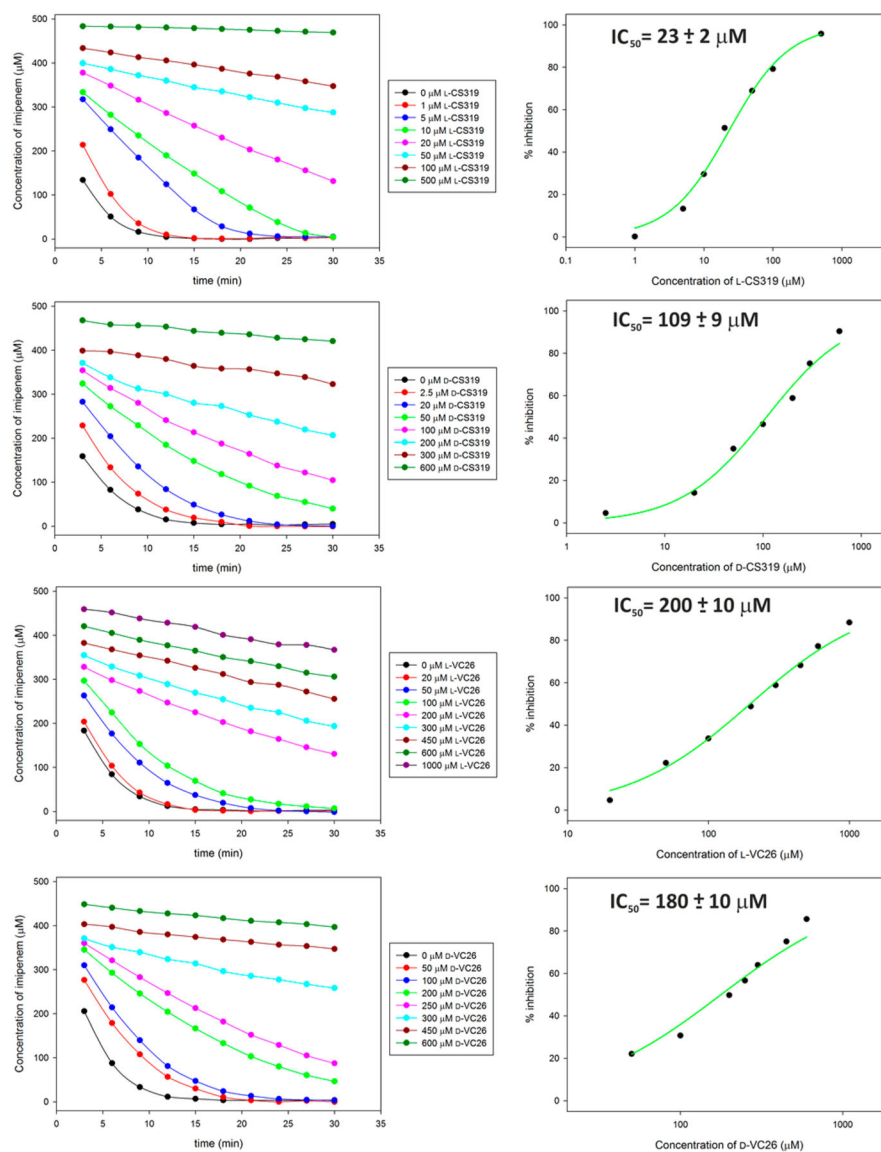
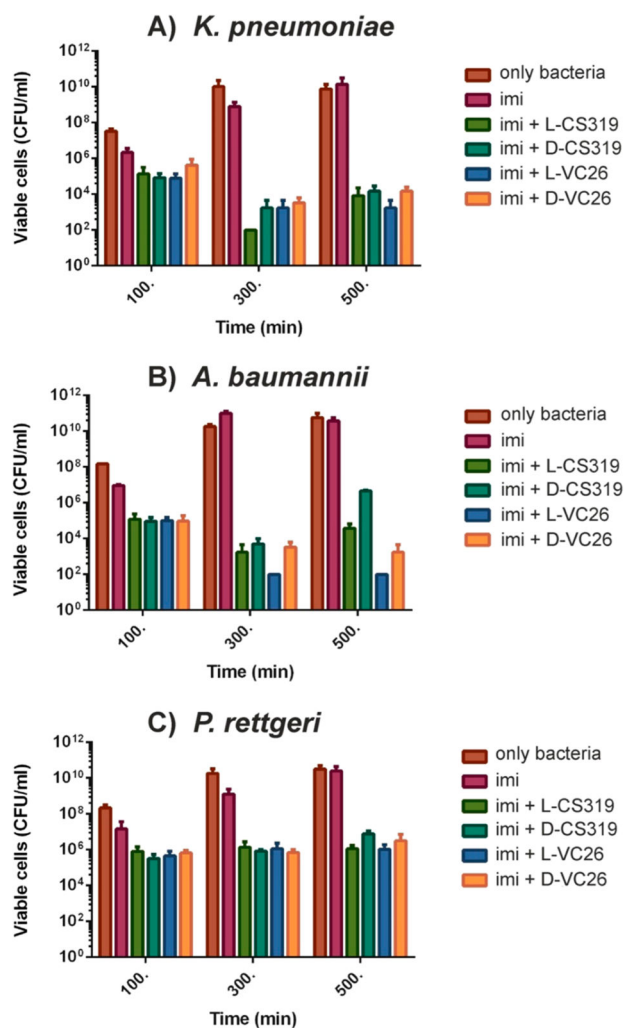


Figure 2. Carbapenem hydrolysis inhibition in *E. coli* cells by BTZs. (Left) Remaining imipenem concentration, as determined from the ¹H NMR spectrum, after a given incubation time with NDM-1-bearing *E. coli* cells, in the absence or in the presence of different concentrations of each bisthiazolidine. (Right) Determination of the IC₅₀ from the plots of the percentage of inhibition as a function of compound concentration using eq 2.

**Figure 3.**

BTZs restore the in vitro activity of imipenem against NDM-1-producing *K. pneumoniae* (A), *A. baumannii* (B), and *P. rettgeri* (C). Bacteria were grown at sublethal concentrations of imipenem alone (4 $\mu\text{g/mL}$ for *K. pneumoniae* and 16 $\mu\text{g/mL}$ for *A. baumannii* and *P. rettgeri*) or in combination with 100 $\mu\text{g/mL}$ of each compound. Viable cells were recovered at 100, 300, and 500 min. Results shown are the mean of three biological replicates \pm SD.

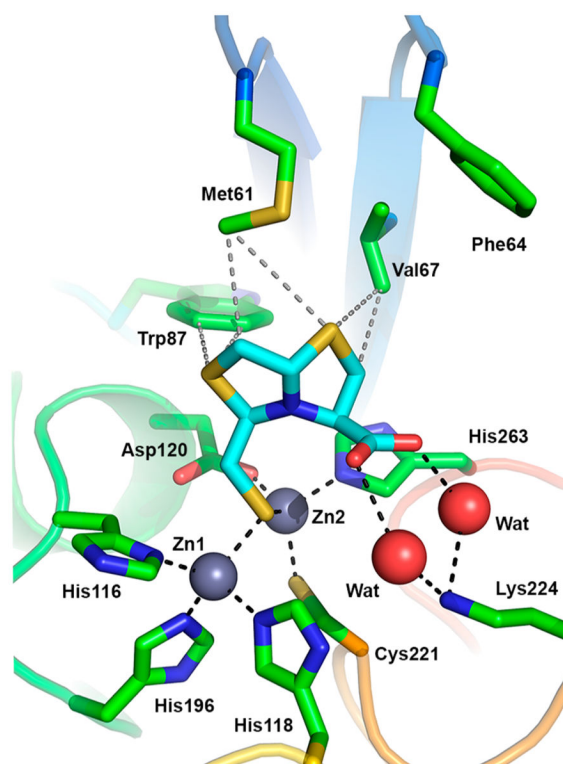


Figure 4.

Crystal structure of the NDM-1:L-CS319 complex. Inhibitor L-CS319 interacts with both zinc ions via its sulfhydryl group. The carboxylate group interacts with K224 through two water molecules (Wats). Zinc ions and water molecules are represented as gray and red spheres, respectively. Hydrogen bonds and zinc coordination bonds are shown as black dashes and hydrophobic interactions as gray dashes. Protein main chain is color-ramped from the N-terminus (blue) to the C-terminus (red). The figure was generated using PyMol (www.pymol.org).

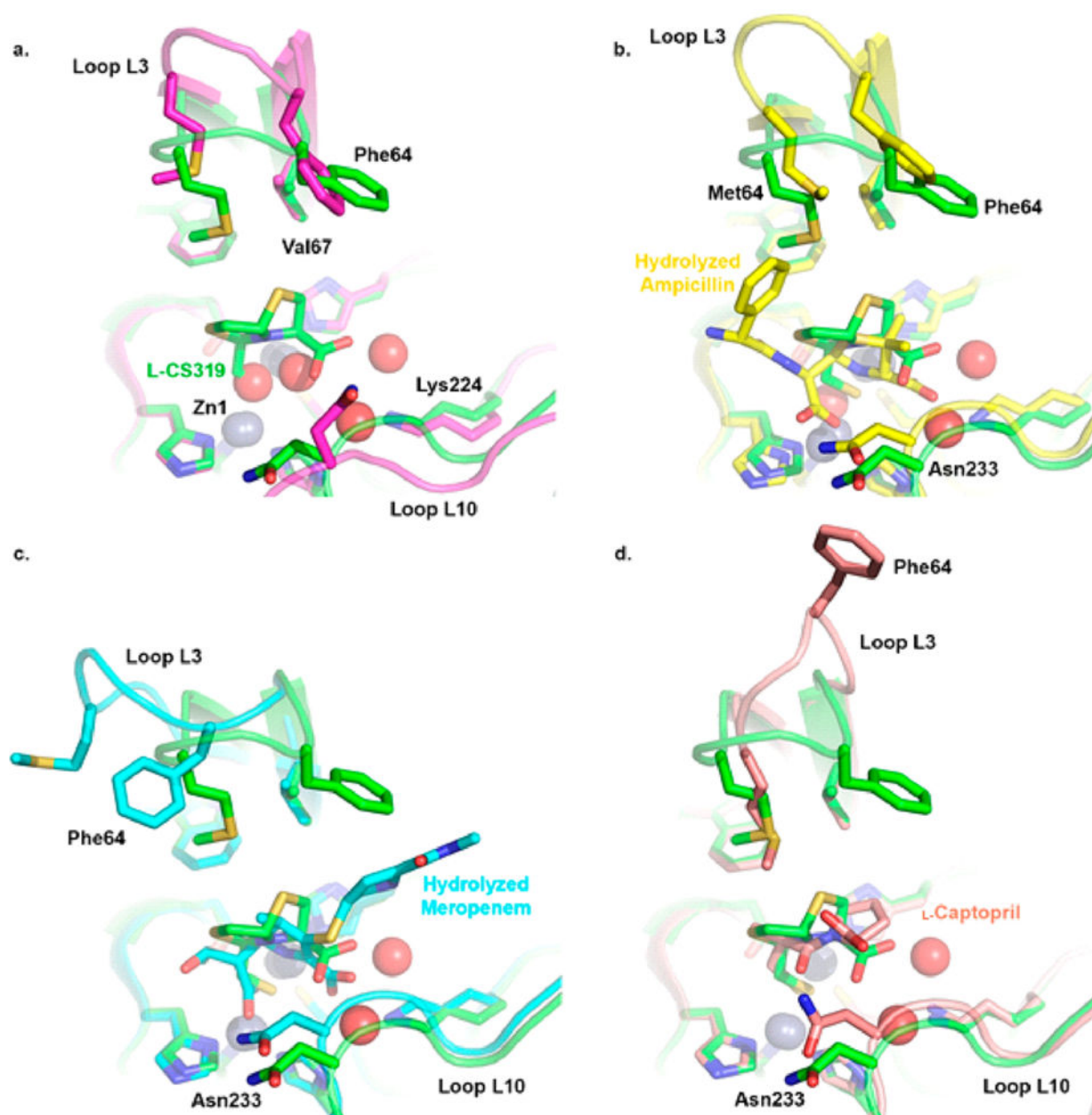
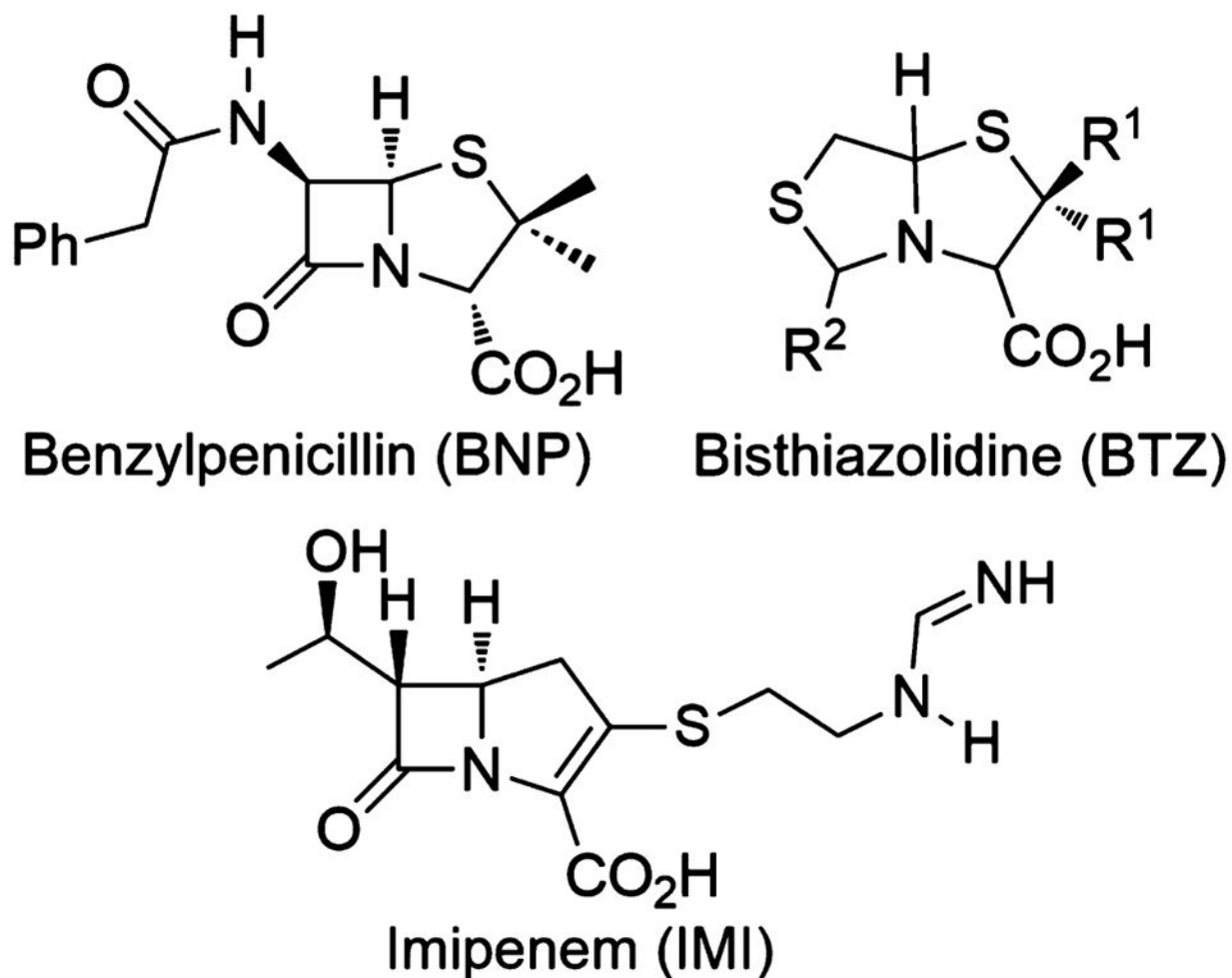


Figure 5.

Comparison of NDM-1:L-CS319 complex with other NDM-1 structures. Overlay of structure of NDM-1:L-CS319 complex (green) with structures of NDM-1: (a) unliganded NDM-1 (magenta, pdb 3SPU); (b) complex with hydrolyzed ampicillin (yellow, pdb 3Q6X); (c) complex with hydrolyzed meropenem (cyan, pdb 4EYL); (d) complex with L-captopril (salmon, pdb 4EXS). Carbon atoms are colored as above, other atoms as standard. Zinc ions (gray spheres) and active site residues from the NDM-1:L-CS319 complex are shown. This figure was generated using Pymol (www.pymol.org).



Scheme 1.
Benzylpenicillin and Imipenem Substrates of NDM-1 and the Bisthiazolidine (BTZ)
Scaffold

Table 1

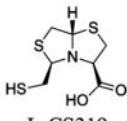
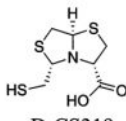
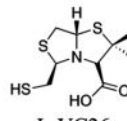
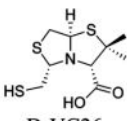
Synthesis of Bisthiazolidines L-CS319, D-CS319, L-VC26, and D-VC26

aminothiols	R ¹	product	yield ^a (%)	dr <i>syn:anti</i> ^b
L-Cys	H	L-CS319	86	95:05
D-Cys	H	D-CS319	80	95:05
L-PNA	Me	L-VC26	89	95:05
D-PNA	Me	D-VC26	76	99:01

^aYields were determined on the basis of isolated pure compounds.^bdr, diastereomeric ratio, was calculated on the basis of ¹H NMR well-defined signals.

Table 2

Inhibition of NDM-1 by Bisthiazolidines

				
L-CS319	D-CS319	L-VC26	D-VC26	
	L-CS319	D-CS319	L-VC26	D-VC26
K_i (μM) ^[a]	7 ± 1	19 ± 3	18 ± 3	12 ± 1
IC ₅₀ (μM) ^[b]	23 ± 2	109 ± 9	200 ± 10	180 ± 10

^[a]Competitive inhibition of NDM-1-catalyzed imipenem hydrolysis by bisthiazolidines.

^[b]IC₅₀ of bisthiazolidines for imipenem hydrolysis by *E. coli* cells expressing NDM-1.

Table 3**Data Collection and Refinement Statistics**

data collection	
processing	XDS/SCALA
beamline	DLS I04-1
space group	P1
cell dimensions (Å)	$a = 46.57$, $b = 69.02$, $c = 69.65$ $\alpha = 87.39^\circ$, $\beta = 88.21^\circ$, $\gamma = 76.75^\circ$
wavelength (Å)	0.9200
resolution ^a (Å)	28.47–1.90 (2.00–1.90)
total reflections ^a	183229 (24469)
unique reflections ^a	62122 (8848)
completeness ^a (%)	93.5 (91.0)
redundancy ^a	2.9 (2.8)
$I/(\sigma I)$ ^a	17.4 (5.4)
R_{merge} ^a (%)	0.045 (0.195)
refinement	PHENIX
total reflections ^a	62116 (2595)
resolution ^a (Å)	27.88–1.90 (1.93–1.90)
R_{cryst} ^a (%)	15.4 (18.7)
R_{free} ^{a,b} (%)	18.2 (24.3)
RMS bond length (Å)	1.179
RMS bond angle (Å)	0.008
protein atoms	6763
water molecules	624
% residues in Ramachandran regions ^c (favored/allowed/disallowed)	98.3/1.7/0
B -factor (protein) ^d	19.6
B -factor (ligand) ^e	33.6
B -factor (water molecules)	29.9
PDB accession code	4U4L

^aData for the highest resolution shell are in parentheses.

^b R_{free} was calculated with 5% of the reflections omitted.

^cCalculated using MolProbity.

^d19.2, 19.2, 18.3, 21.6 for chains A–D, respectively.

^e46.3, 37.0, 34.5, 45.3 for chains A–D, respectively, refined at full occupancy.